# Facile Fabrication of Single-Crystal-Diamond Nanostructures with Ultrahigh Aspect Ratio

*Ye Tao and Christian Degen**

Compatibility with batch fabrication is a technological challenge facing many promising materials for NEMS applications, including carbon nanotubes,[1] graphene nanoribbons,[2,3] nanowires of various material compositions,[4,5] and single-crystal diamond. Often, multiple reasons prevent a promising material system from "going batch", such as low yield during material synthesis, difficulty in controlling geometry, placement, and orientation during growth and processing, as well as poor consistency in the quality of finished devices. Single-crystal diamond is one of such promising materials with unparalleled material properties, which have not yet been fully unlocked due to difficulties associated with its growth and processing.[6–9]

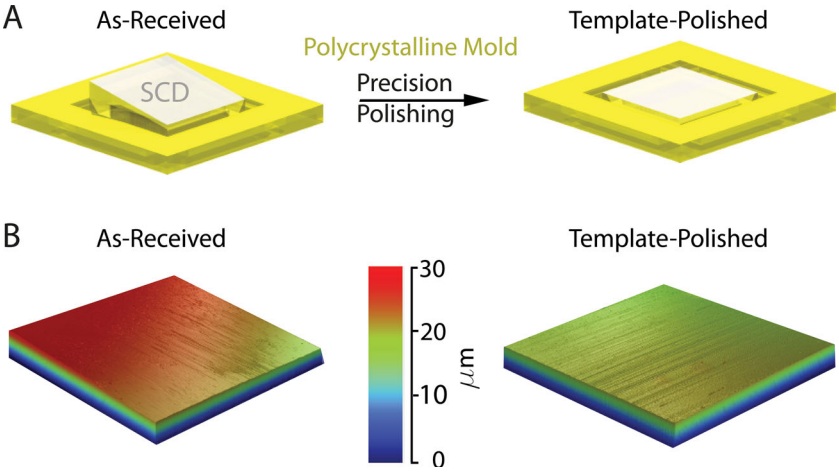


**Figure 1.** Template polishing of single-crystal diamond (SCD) sheets. A) An initially wedged sample is embedded into a polishing mold made of polycrystalline diamond and subjected to mechanical polishing until level with the rim of the mold. B) Representative profilometer scan images of SCD sheets before and after precision polishing.

These difficulties are unfortunate because diamond holds fascinating promise for many cutting-edge fields of research. Its exceptional mechanical properties are poised to boost efforts in force sensing and optomechanics by a simple exchange of device material.[10–12] The wide optical transparency window and high refractive index are ideal for plasmonic and photonic structures that may be integrated in optical networks.[13] Purposely created lattice impurities and defects, such as the nitrogen-vacancy (NV) center, hold promise for single photon generators and ultrasensitive detectors for magnetic fields under ambient conditions.[14–17] Progress toward such integrated and high-quality diamond devices would be greatly accelerated by the availability of methods for the batch-fabrication of single-crystal diamond.

The main reason that makes diamond nanofabrication difficult is the fact that single-crystal diamond cannot be grown heteroepitaxially. In other words, no wafers with a single-crystal diamond device layer are currently available. As a result, obtaining high-quality starting material that facilitates subsequent device elaboration becomes the central challenge. Chemical-vapor-deposited (CVD) diamond, the highest-quality material currently grown in industrial processes, is limited in size to <10 × 10 mm (more typically <4 × 4 mm) plates at a thickness of several hundred micrometers. This starting material must be subsequently micromachined and lithographically processed to arrive at the desired MEMS or NEMS device.

Existing strategies for making single-crystal diamond nanostructures can be roughly divided into three categories based on the nature of the starting material. In no particular order, category A is the fabrication of devices directly on the top surface of a thick, polished single crystal. Methods employed so far include direct FIB machining,[8] creation of a suspended surface layer from bulk diamond via implantation damage to an underlying sacrificial layer followed by its selective removal,[6,9,18,19] and transferring of ebeam-defined resist structures to the bulk diamond by angled anisotropic plasma etching.[20] Category B relies on heteroepitaxial polycrystalline diamond films with large grain size. Although polycrystalline, this material can still exhibit single-crystal quality if the relevant device dimensions are substantially smaller than the grain size.[21] Here, suitable substrate layers, specialized nucleation techniques, and sufficient growth time lead to a thick polycrystalline film (>10 μm) with characteristics of a dislocation-rich single-crystal at the top surface.[22] Following diamond growth and mechanical polishing of the top surface, the supporting substrate and the bulk part of the epitaxial film need to be removed from the backside via plasma etching steps to provide a suspended device layer. The advantage of this method is the possibility of

Y. Tao, Prof. C. Degen
Department of Physics
ETH Zurich, Schafmattstrasse 16,
8093 Zurich, Switzerland
Phone: +41 44 633 23 36; Fax: +41 44 633 10 56
E-mail: degenc@ethz.ch
Y. Tao
Department of Chemistry
Massachusetts Institute of Technology
77 Massachusetts Avenue, Cambridge MA 02139, USA

**DOI: 10.1002/adma.201301343**

growing wafers up to several inches in diameter, while the disadvantage is that single-crystal areas are restricted to the grain size and may not be suitable for larger devices. Category C, finally, employs commercially available single-crystal plates that are laser-sliced and polished down to 10–40 µm thickness by the manufacturers. These diamond sheets are then further thinned by extensive plasma etching to the desired device layer thickness and structures, defined by standard lithographic methods.[23,24]

Category C holds several key advantages for enabling batch processing and general usage and is the route of choice in this paper. It is currently the only approach for making large-area (millimeter-sized) structures that avoids ion bombardment (category A) and grain boundaries (category B). Furthermore, fabrication can be carried out without the need for specialized equipment or processes other than those available in standard cleanrooms. Given the large initial thickness of the diamond plates used in this approach (tens of micrometers) compared to the typical device layer thickness with common wafers (hundreds of nanometers), several technical hurdles will still need to be overcome to advance diamond nanofabrication to a level similar to, say, that of silicon. The first hurdle is a method for producing uniformly thick plates with a sub-micrometer wedge over millimeter-size lateral dimensions. The second hurdle is finding simple and robust methods for forming a strong and stable bond between the single-crystal diamond plate and an arbitrary handling substrate. Finally, for very thin devices (≲100 nm), etch processes must be very uniform and methods need to be developed to monitor the thickness of such samples precisely.

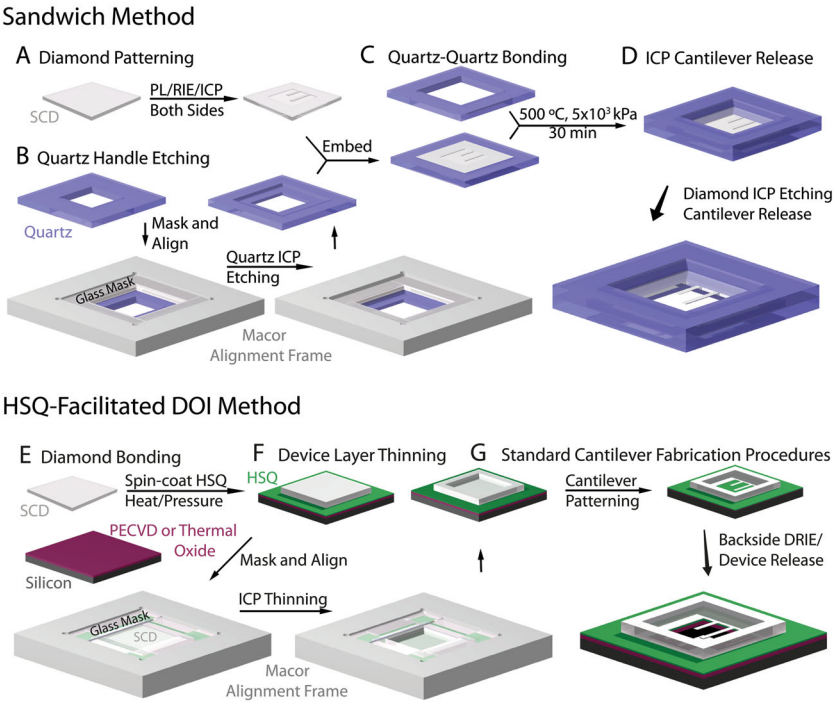


**Figure 2.** Outline of the "Sandwich" and "DOI" (diamond-on-insulator) methods for single-crystal diamond (SCD) NEMS fabrication. A) In the "sandwich method", diamond sample is patterned with cantilevers on the front side and a 5 µm-deep pit on the back side to serve as mechanical support for released cantilevers. B) The quartz handle is prepared for diamond sandwiching by ICP etching a square receptacle to accommodate the diamond plate and to allow direct contact of the two mating quartz slides. A macor frame is used to align glass masks to the quartz slide during ICP etching. C) After placing the diamond plate within the receptacle pit, quartz slides are brought into contact and subjected to thermo-pressure wafer bonding, resulting in a "sandwich" structure. D) Devices are released by a long ICP etch from the back side by removing excess diamond material. E) In the "DOI method", diamond sheet is wafer-bonded to a handling substrate, in this example a silicon wafer bearing a SiO layer, via spin-coated HSQ interlayer. F) Diamond device layer is thinned down to desired cantilever thickness by ICP etching while masked by glass mask, positioned over the sample with the aid of a macor alignment frame. G) Fully released diamond cantilevers are fabricated following standard procedures as known for DOI and SOI wafers.[27]

Here, we present a protocol to easily shape commercially available single-crystal-diamond plates into diamond NEMS with thickness down to below 100 nm and lateral dimensions up to several hundred micrometers, thus achieving aspect ratios over 2000. The protocol features a template-assisted precision repolishing step for achieving high thickness uniformity, two independent wafer-bonding strategies, and final device elaboration using standard lithography and plasma etching. We demonstrate these processes by fabricating single-crystal diamond nanocantilevers with thicknesses between 50–800 nm and lengths up to 240 µm. We have recently found that such cantilevers exhibit exceptional mechanical quality factors exceeding one million at room temperature.[25] We conclude with a discussion of the prospects and the limitations of the presented methods for making even thinner, higher-aspect-ratio structures, and for extending fabrication toward integrated, three-dimensional structures.

Our starting point for fabricating MEMS and NEMS devices are commercially-available single-crystal diamond plates grown by chemical vapor deposition (CVD). These plates can be grown at extraordinarily high purity and with low internal strain, which is important for many applications. Plates are typically laser-cut and polished to a lateral size of several mm, thickness between 10–50 µm, and a surface roughness ~1 nm-rms. As the polishing step is difficult to control precisely, plates usually exhibit large wedges, with thickness variations often exceeding 10 µm across a plate. This thickness variation is a major hurdle when fabricating sub-micrometer structures, as it is directly transferred onto the device layer when the material is further thinned by uniform plasma etching.

To overcome this hurdle, we have devised a template-based polishing strategy that allowed us to consistently reduce the wedge across plates to below 0.5 µm per mm. Our approach is illustrated in **Figure 1**A: the original diamond plate is fixed by glue in the central pit of a larger polycrystalline diamond support wafer. This pit was created by plasma-etching, with a depth less than the diamond plate thickness (typ. 10–20 µm)



*Adv. Mater.* **2013**,
DOI: 10.1002/adma.201301343

and lateral dimensions slightly larger than (but similar to) those of the diamond plate. The diamond plate thus protrudes beyond the polycrystalline diamond wafer. Upon polishing, the material from the single crystal plate is thus removed first. Moreover, owing to the better mechanical wear resistance of polycrystalline diamond compared to <100> single crystals,[26] material removal essentially comes to a halt as the polycrystalline surface is reached. The released diamond plate then has a thickness set by the depth of the polycrystalline mold, and a thickness uniformity given by the initial uniformity of the pit. Since the pit is created by plasma etching, which can be made very uniform, very flat plates result.

Representative profilometer scan images are shown in Figure 1B, with additional data given as Supporting Information. These measurements showed an average improvement in thickness uniformity from 6.6 ± 2.5 μm (1.5 ± 0.5 μm/mm) for as-received material to 1.4 ± 1.0 μm (0.3 ± 0.2 μm/mm) for re-polished plates. Complementary measurements of the etched pit showed a depth variation of about 1 μm, suggesting that the final plate thickness variation was caused by non-uniform plasma etching of the mold. Uniformity of the plasma etching could be significantly improved by periodically rotating the polycrystalline diamond template during the etch process; for this study, the template wafer was simply placed in the ICP etcher and processed in a single etching step without any sample rotation. It should thus be possible to directly improve thickness uniformity beyond the already decent ~0.3 μm/mm achieved with first-generation molds. In fact, we have achieved <20 nm/mm depth variation in our newest batch of polycrystalline molds.

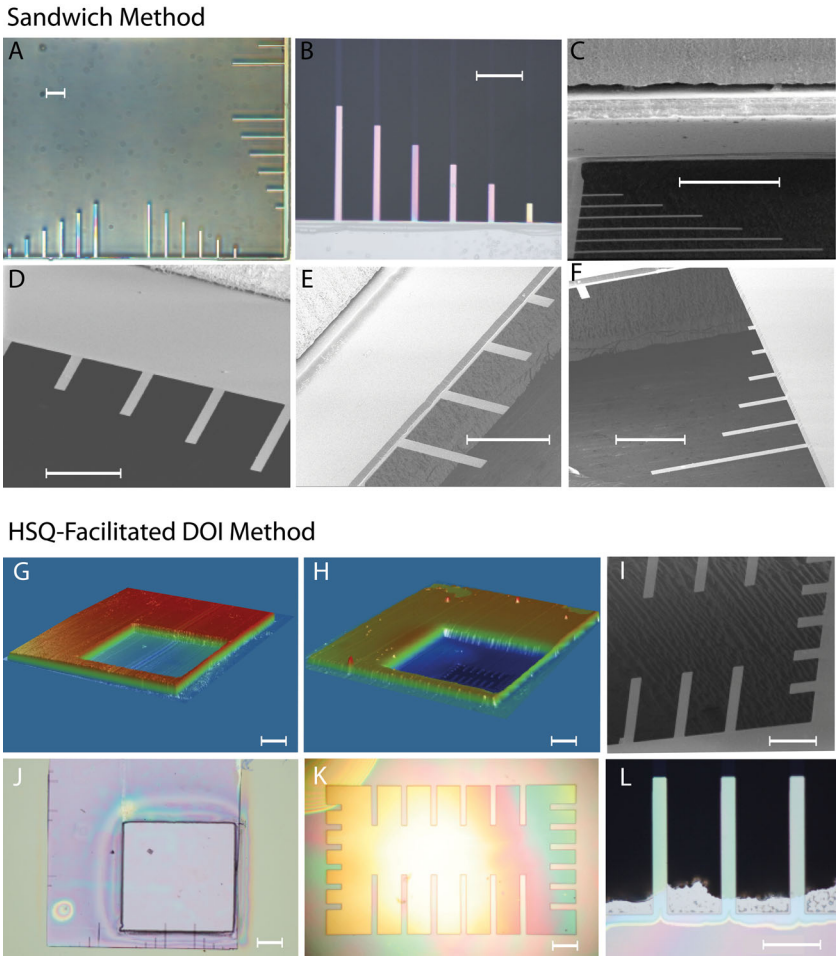


**Figure 3.** Representative optical, SEM, and profilometry images of devices. A–F) Optical and SEM images of diamond cantilevers fabricated using the sandwich method. Scale bars are 100 μm. G-H are profilometry, I is an SEM, and J-L are optical images of a DOI sample during device elaboration and after wafer bonding. G and J: After Device Layer Thinning step (as in Figure 2F). H and K: Before backside patterning and etching. In this sample, the diamond has been covered with a layer of PECVD oxide and nitride for protection during backside processing. I and L: After device release step (as in Figure 2G). Scale bars are 200 μm (G, H, J) and 50 μm (I, K, L).

In a next step, we describe two facile wafer-bonding processes to bond the diamond sheet to arbitrary substrates, most notably silicon and quartz. A bonded diamond plate can then be handled and further processed like any conventional device layer on a carrier wafer. In a first, more specialized approach, we explored clamping of the repolished diamond sheet between two thermally-fused quartz slides, resulting in a quartz-diamond-quartz sandwich structure (**Figure 2**). In this way, the diamond plate remains accessible from both sides, which facilitates fabrication of membrane-like MEMS or NEMS structures. Moreover, quartz can be used both as a convenient handling and mask material. (We note that while quartz was used as the substrate here, many other materials, such as sapphire, would be equally suited or even superior substrates.) Moreover, the dual use of the quartz substrates saves several mask deposition and patterning steps and provides a few further advantages that are discussed in more detail later.

The second approach explored involved direct bonding of diamond sheets to an oxide-bearing silicon carrier wafer using hydrogen silsesquioxane (HSQ) resist as the bonding agent. HSQ is a flowable oxide that converts into silicon dioxide under thermal annealing, resulting in a generic diamond-on-insulator (DOI) substrate. The basic bonding steps are shown in Figure 2: We first cleaned the diamond film in a boiling piranha solution, followed by DI water rinsing, air drying, and a 5-minute dehydration bake at 200 C. We spin coated the oxide wafer chip (thermal or PECVD) with HSQ for 10 seconds at 2000 RPM. The diamond film was deposited onto the HSQ-coated surface at the desired location. Sturdy bonding developed after 30 minutes under pressures >10 kPa and at 500 Celsius. We emphasize that hydrophilic surfaces are essential for bonding. While we have also tested several existing methods for producing DOI substrates,[23,24,28] we have found HSQ-mediated bonding to be particularly robust and to show a high tolerance

towards surface roughness and undulations. The fluid and slightly moldable nature of the HSQ interlayer has given essentially 100% success rate for mating surfaces having up to 10 nm-rms roughness. Secondly, we found it possible to bond diamond sheets that are buckled, wrinkled, or that have kinks on the surface. For the latter, it is essential to use a soft interlayer between the bonding platen, such as graphite wafers, that can elastically deform. Lastly, we found the resulting bond to be extremely stable. Extended soaking in 49% HF, sometimes overnight for large samples (>4 mm), were necessary to dislodge a bonded diamond sheet.

In a last fabrication step, the bonded diamond sheet is either fully etched away to release pre-patterned devices (Sandwich Method, Figure 2D) or thinned to sub-micrometer thickness using Ar/Cl-based ICP etching[29,30] (DOI Method, Figure 2F). The thinning process uses glass or quartz mask to shield the outer portions of the DOI substrate and is held in place by a macor alignment frame. Thickness of the bonded diamond sheet was monitored after each cycle of ICP etching by profilometer scans across the sample. Once the film was thinned down to the desired sub-micrometer thickness, standard lithographic fabrication procedures[27] were used to yield, after front- and backside patterning and etching steps, fully released cantilever test devices (Figure 2G).

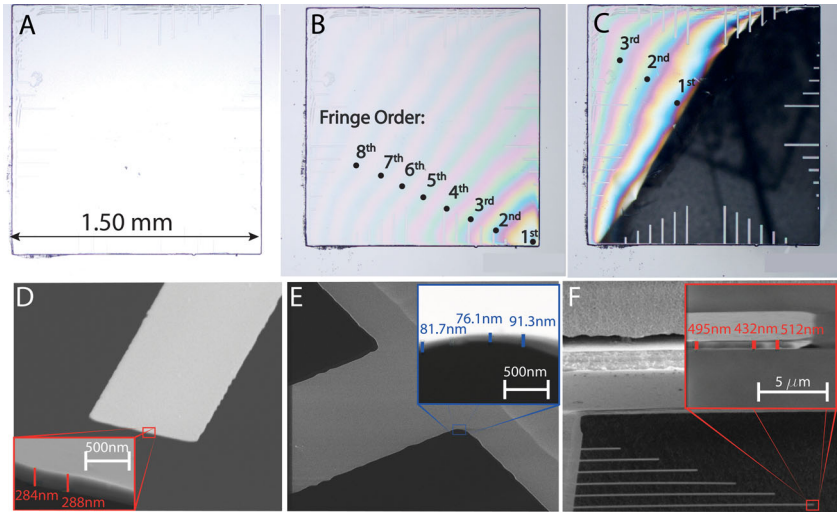


**Figure 4.** Methods for determining thickness of diamond membrane and cantilever devices. A-C) Optical microscopy images of the initial diamond plate (A, thickness ~10 μm), with the thickness of the membrane reduced by ICP etching to ~1 μm (B), and with an additional thickness reduction of ~0.8 μm (B). Successive green fringes are marked by fringe order and are separated in thickness by 110(8) nm. D-F) Examples of SEM images used to measure thicknesses of diamond cantilevers.

**Figure 3** collects a series of optical, scanning electron microscope, and profilometer images of intermediate and finished devices. Four batches were prepared during the course of this study, with an overall yield of released cantilevers after ICP etching of >98% (over 100 devices were fabricated).

**Figure 4** illustrates that device thickness <100 nm can be achieved and that thickness can be precisely controlled. We employed three independent methods for monitoring thickness of devices during thinning: Optical thin-film interferometry, scanning electron microscopy (SEM), and measurements of mechanical resonance frequencies combined with theoretical modeling. Figure 4A–C shows optical microscopy images of a diamond sheet before, during, and after device release by ICP etching. We noticed that an interference pattern becomes visible as the membrane thickness is reduced to below around 1 μm, with a thickness difference of 110(8) nm between two green fringe maxima. We found the diamond etch rate to be well reproduced using fringe-based thickness estimation. For example, fringes receded by about 7 orders between Figure 4B and 4C, corresponding to a thickness reduction by 770 ± 56 nm using 20 min of etching. This is in good agreement with the calibrated etch rate of 840 ± 60 nm per 20 min (see Table 1 in Supporting Information). To confirm the interference measurements, we have also determined the thicknesses of several cantilevers at the tip and and the base using SEM images (Figure 4). We found good agreement for thicker devices, but found SEM measurements to systematically yield smaller thickness values for thin (<200 nm) devices. Moreover, we compared thickness data to measured values of mechanical resonance frequencies combined with numerical calculations (Comsol), and found those data to be in excellent agreement with the optical interference measurements. We thus believe that the optical data are the most precise, and suspect the systematic errors in SEM thickness measurements to come from charging effects and limited imaging resolution. Overall, we estimate the error in fringe-based thickness estimation to be <30 nm.

In an attempt to further reduce the thickness of devices, we have subjected fully released, free-standing nanocantilevers to additional ICP etching. While not all devices survived this ICP and the following cleaning process, some of the resulting cantilevers showed thicknesses between 40–50 nm (see **Figure 5**). As can be seen from the figures, smallest dimensions occurred near the base of the devices. The thickness variation may be both due to the residual wedge from the polycrystalline diamond polishing mold, or due to non-uniform etching in the ICP. We note that most cantilevers in this additional thinning process were actually lost while drying them from the post-etching IPA rinse; we did not have access to a critical-point dryer (CPD) at the time of the experiment and just pulled the cantilever sample out from liquid IPA. Thus, we expect that ICP etching would support even thinner structures.

In summary, we have presented two robust and facile methods for fabricating single-crystal diamond NEMS and MEMS devices. Two key technical innovations were presented. Firstly, a novel polishing approach based on a polycrystalline diamond mold template enabled the achievement of sub-micrometer thickness uniformity in bulk diamond plates. Secondly, two wafer bonding methods were presented, including quartz-diamond-quartz sandwich structures and HSQ-mediated diamond-on-insulator substrates with a silicon



Adv. Mater. 2013,
DOI: 10.1002/adma.201301343

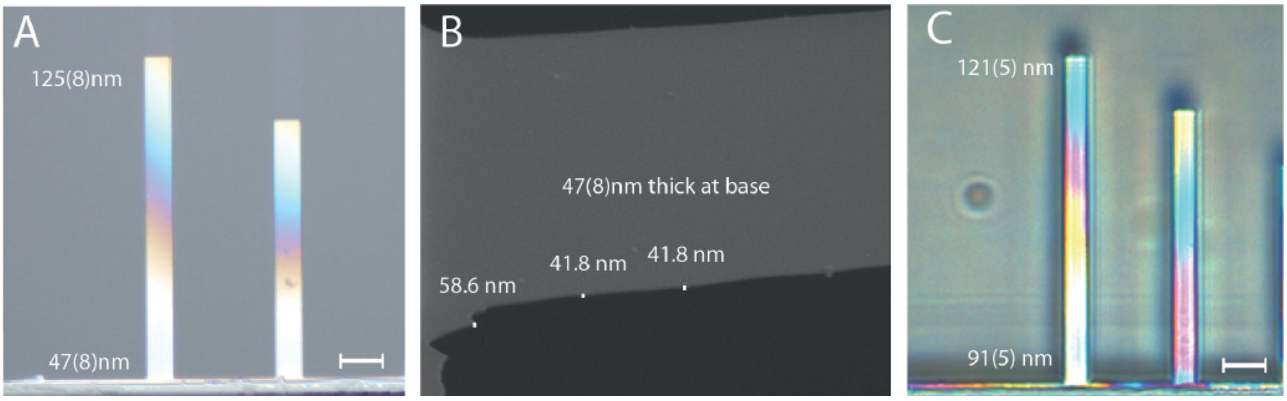


**Figure 5.** Thinnest devices fabricated in this study using a second ICP etching step. A) Optical image of two sub-100-nm thick cantilever devices. The longer cantilever is 240 µm in length and has a thickness of 47(8) nm at the base and 125(8) nm at the tip, respectively. B) Scanning electron microscopy image of the same cantilever, measuring a base thickness of about 50 nm. C) Optical image of two other cantilever devices exhibiting a sub-100-nm thickness at the base. Scale bars are 20 µm.

carrier wafer. Both methods could be easily extended to other substrate materials, such as sapphire. Furthermore, both methods are versatile starting points for further refinement in diamond device fabrication: The sandwich method, for example, is ideally suited for fabricating more complex, three-dimensional structures due to the dual-side access to the diamond layer. One could envisage making sharp AFM tips,[31] mass-loading,[27] or optical microlenses[32] on one side of the diamond sheet before patterning and releasing the cantilever by etching from the opposite side. The DOI method, on the other hand, could be easily combined with ion implantation and homoepitaxial regrowth[9,33] as an alternative to laser-cut, re-polished, and etch-thinned diamond plates. We have exemplified the capabilities of the methods presented in this study by lithographically fabricating nanocantilevers with extreme aspect ratios (over 2000:1), including device thicknesses down to 50 nm and lengths up to 240 µm. Given the extreme mechanical strength of the material, reflected in an almost 100% yield of finished devices, there is considerable scope that single-crystal diamond structures with even more extreme aspect ratios may be feasible. In the absence of a method for heteroepitaxially growing single-crystal diamond, we believe that the methods reported herein provide a promising platform for enabling single-crystal diamond NEMS and MEMS fabrication for high-end research and industrial applications.

## Acknowledgements

We acknowledge funding by the Swiss National Science Foundation (through SNSF grant 200021_137520/1 and the NCCR QSIT). We thank Joseph Tabeling, Peter Morton and the technical staff at DDK for assistance with diamond polishing and Matthew Markham at ElementSix for providing diamond samples through the DARPA QuASAR program. We thank the clean room staff at FIRST Lab and CLA (ETH), IBM Zurich, and the MTL at MIT for advice on fabrication. We thank Kurt Broderick, Ute Drechsler, Mona Klein, Paolo Navaretti, Donat Scheiwiller, and Dave Webb for technical assistance and useful discussions.

Received: March 25, 2013
Published online:

[1] V. Sazonova, Y. Yaish, H. Üstünel, D. Roundy, T. A. Arias, P. L. McEuen, *Nature* **2004**, *431*, 284.
[2] X. Li, X. Wang, L. Zhang, S. Lee, H. Dai, *Science* **2008**, *319*, 1229.
[3] L. C. Campos, V. R. Manfrinato, J. D. Sanchez-Yamagishi, J. K. P. Jarillo-Herrero, *Nano Lett.* **2009**, *9*, 2600.
[4] S. M. Tanner, J. M. Gray, C. T. Rogers, K. A. Bertness, N. A. Sanford, *Appl. Phys. Lett.* **2007**, *91*, 203117.
[5] S. Perisanu, P. Vincent, A. Ayari, M. Choueib, S. T. Purcell, M. Bechelany, D. Cornu, *Appl. Phys. Lett.* **2007**, *90*, 043113.
[6] P. Olivero, S. Rubanov, P. Reichart, B. Gibson, S. Huntington, J. Rabeau, A. D. Green-tree, J. Salzman, D. Moore, D. Jamieson, S. Prawer, *Diam. Relat. Mater.* **2006**, *15*, 1614.
[7] B. A. Fairchild, P. Olivero, S. Rubanov, A. D. Greentree, F. Waldermann, R. A. Taylor, I. Walmsley, J. M. Smith, S. Huntington, B. C. Gibson, D. N. Jamieson, S. Prawer, *Adv. Mater.* **2008**, *20*, 4793.
[8] B. Z. Kupfer, R. K. Ahmad, A. Zainal, R. B. Jackman, *Diam. Relat. Mater.* **2010**, *19*, 742.
[9] I. Aharonovich, J. C. Lee, A. P. Magyar, B. B. Buckley, C. G. Yale, D. D. Awschalom, E. L. Hu, *Adv. Mater.* **2012**, *24*, OP54.
[10] D. Rugar, R. Budakian, J. H. Mamin, B. W. Chui, *Nature* **2004**, *430*, 329.
[11] C. L. Degen, M. Poggio, H. J. Mamin, C. T. Rettner, D. Rugar, *Proc. Nat. Acad. Sci. USA* **2009**, *106*, 1313.
[12] J. C. Sankey, C. Yang, B. M. Zwickl, A. M. Jayich, J. G. E. Harris, *Nat. Phys.* **2010**, *6*, 707.
[13] I. Aharonovich, A. D. Greentree, S. Prawer, *Nat. Photonics* **2011**, *5*, 397.
[14] C. L. Degen, *Appl. Phys. Lett.* **2008**, *92*, 3243111.
[15] P. Maletinsky, S. Hong, M. S. Grinolds, B. Hausmann, M. D. Lukin, R. L. Walsworth, M. Loncar, A. Yacoby, *Nat. Nanotechnol.* **2012**, *7*, 320.
[16] H. J. Mamin, M. Kim, M. H. Sherwood, C. T. Rettner, K. Ohno, D. D. Awschalom, D. Rugar, *Science* **2013**, *92*, 557.
[17] T. Staudacher, F. Shi, S. Pezzagna, J. Meijer, J. Du, C. A. Meriles, F. Reinhard, J. Wrachtrup, *Science* **2013**, *339*, 561.
[18] M. Liao, C. Li, S. Hishita, Y. J. Koide, *Micromech. Microeng.* **2010**, *20*, 085002.
[19] M. K. Zalalutdinov, M. P. Ray, D. M. Photiadis, J. T. Robinson, J. W. Baldwin, J. E. But-ler, T. I. Feygelson, B. B. Pate, B. H. Houston, *Nano Lett.* **2011**, *11*, 4304.
[20] M. J. Burek, N. P. de Leon, B. J. Shields, B. J. M. Hausmann, Y. Chu, Q. Quan, A. S. Zi-brov, H. Park, M. D. Lukin, M. Loncar, *Nano Lett.* **2012**, *12*, 6084.

[21] K. D. Jahnke, B. Naydenov, T. Teraji, S. Koizumi, T. Umeda, J. Isoya, F. Jelezko, *Appl. Phys. Lett.* **2012**, *101*, 012405.
[22] J. Riedrich-Möller, L. Kipfstuhl, C. Hepp, E. Neu, C. Pauly, F. Mücklich, A. Baur, M. Wandt, S. Wolff, M. Fischer, S. Gsell, M. Schreck, C. Becher, *Nat. Nanotechnol.* **2012**, *7*, 69.
[23] A. Faraon, P. E. Barclay, C. Santori, K.-M. C. Fu, R. G. Beausoleil, *Nat. Photonics* **2011**, *5*, 301.
[24] B. J. M. Hausmann, B. Shields, Q. Quan, P. Maletinsky, M. McCutcheon, J. T. Choy, T. M. Babinec, A. Kubanek, A. Yacoby, M. D. Lukin, M. Loncar, *Nano Lett.* **2012**, *12*, 1578.
[25] Y. Tao, J. M. Boss, B. A. Moores, C. L. Degen, *arXiv:1212.1347* **2012**.
[26] N. Dubrovinskaia, S. Dub, L. Dubrovinsky, *Nano Lett.* **2006**, *6*, 824.
[27] B. W. Chui, Y. Hishinuma, R. Budakian, H. J. Mamin, T. W. Kenny, D. Rugar, The 21th International Conference on Solid State Sensors, Actuators and Microsystems **2003**, 1120.
[28] P. Ovartchaiyapong, L. M. A. Pascal, B. A. Myers, P. Lauria, A. C. B. Jayich, *Appl. Phys. Lett.* **2012**, *101*, 163505.
[29] C. L. Lee, E. Gu, M. D. Dawson, I. Friel, G. A. Scarsbrook, *Diam. Relat. Mat.* **2008**, *17*, 1292–1296.
[30] B. J. Hausmann, M. Khan, Y. Zhang, T. M. Babinec, K. Martinick, M. McCutcheon, P. R. Hemmer, M. Loncar, *Diam. Relat. Mat.* **2010**, *19*, 621–629.
[31] A. Malavé, E. Oesterschulze, *Rev. Sci. Instrum.* **2006**, *77*, 043708.
[32] C. Lee, E. Gu, M. Dawson, I. Friel, G. Scarsbrook, *Diam. Relat. Mater.* **2008**, *17*, 1292.
[33] C. F. Wang, E. L. Hu, J. Yang, J. E. J. Butler, *Vac. Sci. Technol. B* **2007**, *25*, 730.



*Adv. Mater.* **2013**,
DOI: 10.1002/adma.201301343

**Supplementary Information**

# Facile Fabrication of Single-Crystal-Diamond Nanostructures with Ultra High Aspect Ratio

By Ye Tao[†,‡] and Christian Degen[†]

[†] *Dept. of Physics, ETH Zurich, Schafmattstrasse 16, 8093 Zurich, Switzerland.*
[‡] *Dept. of Chemistry, Mass. Institute of Technology, 77 Mass. Ave.,Cambridge MA 02139, USA.*

## 1) General experimental notes:

In all ICP etching performed in this study, quartz carrier wafers was used in place of the usual silicon carrier wafer. This change was necessary because of the relatively high etch rate of silicon in the $Ar/Cl_2$ plasma (300nm/min) that would have led to contamination of both the diamond sample and the ICP chamber by the sheer quantity of released volatile and non-volatile etch products.

Table 1: ICP Etching Recipes For Materials Used in Study

| Parameter | Diamond | Quartz | Sapphire |
|---|---|---|---|
| Ar Flow (sccm) | 5 | 50 | 10 |
| $Cl_2$ Flow (sccm) | 10 | 0 | 0 |
| $SF_6$ Flow (sccm) | 0 | 50 | 0 |
| $BCl_3$ Flow (sccm) | 0 | 0 | 90 |
| Pressure (mtorr) | 1.0 | 10 | 10 |
| ICP Power (W) | 500 | 1000 | 100 |
| Bias Power (W) | 200 | 200 | 200 |
| Temperature (°C) | 50 | 50 | 50 |
| Etch Rate (um/h) | 2.8 | 30 | 23 |

Table 2: Template Precision Polishing, Results

| Sample | Thickness Variation (As-Received) ($\mu$m) | Thickness Variation (After Precision Polishing) ($\mu$m) |
|---|---|---|
| 1 | 5.76(13) | 1.25(10) |
| 2 | 10.65(5) | 0.50(7) |
| 3 | 6.45(12) | 2.47(7) |

## 2) Fine Details of the Sandwich Method:

We initiated the ``Sandwich method" by removal of mechanical polishing damage on the sample surface by etching away 200 nm of material from the top side of the diamond film in a $Ar/Cl_2$ ICP plasma. (Etching parameters are collected in Table 1). Devices were patterned on the same side via standard photolithography (PL) and plasma etching steps, using stress-free PECVD silicon oxide-silicon nitride alternating layers as the hardmask (300 nm in total). Device patterns were transferred into the diamond to a depth of 800 nm - 900 nm via cyclic $O_2$ and $O_2/CF_4$ reactive ion etching (RIE). These depths ensured that released structures would be sub-micron in thickness. After front-side patterning, the diamond film was turned upside-down and a 5 um-deep square pitted frame having the same lateral dimension as the perimeters of the front-side pattern was etched into the back side surface

using $Ar/Cl_2$ plasma. The edges of the square were aligned to the base of cantilevers on the front-side pattern so that the 5-um-thick perimeter would serve as a clamping mass at the base of the cantilevers once they are released in an ICP etching step later. Hardmask used in this clamping-mass patterning step was a 5 um, stress-free, alternating layers of $SiO_2$ and $Al_2O_3$ deposited by e-beam evaporation and liftoff (Figure 2A). After a HF wet etching to remove any residual hardmask and a short piranha cleaning to remove any residual organic contaminants, the diamond film was ready for sandwiching.

We proceeded to prepare the quartz (or sapphire) handles for sandwiching by first laser-cutting (Laser Micromachining Ltd.) square through-holes on the dies (Figure 2B). The size of the through holes was adjusted to be larger than the perimeter of the diamond pattern by at least 200 um on each side, while still smaller than the lateral dimensions of the diamond film. Next, a pit with dimensions slightly larger than those of the diamond film was etched into the quartz, fully spanning and encompassing the through hole. We found that a convenient and expedient method is to use a shadow mask pieced together using diced glass microscope cover slides (Figure 2B). We ensured alignment of the shadow mask to the substrate using a macor alignment frame during ICP machining. 20-um-deep diamond receptacle pit can be efficiently machined in about 40 minutes using a $SF_6$ based or a $BCl_3$ based ICP plasma on quartz and sapphire handle slides.

Right before sandwiching, we cleaned both the top and bottom handle slides for 10 minutes in a boiling piranha solution, followed by DI water rinses and drying under nitrogen flow. We nudged the diamond sheet into the receptacle pit and completed the sandwich with the upper slide (Figure 2C). We loaded the assembly into a wafer bonder and performed wafer bonding at a temperature of 500 $^0$C and a pressure of 5,000 kPa for 30 minutes. After wafer bonding, the quartz-quartz or sapphire-sapphire interface became fused and optically invisible. The sample chip is cleaned again in a piranha solution before loading into the ICP for diamond bulk thinning and concurrent cantilever release (Figure 2D). The progress of the thinning and release can be conveniently followed by ellipsometry, using an air-diamond-air model. Under the microscope, colorful optical thin-film interference fringes become apparent on the residual diamond film once its thickness has been reduced below 1um. ICP etching was continued until the cantilevers were completely freed from the supporting diamond membrane.

**3) Comparison of SEM and Optical Interometry Device Thicknesses**